

CurbNet: Curb Detection Framework Based on LiDAR Point Cloud Segmentation

Guoyang Zhao¹, Fulong Ma¹, Yuxuan Liu², Weiqing Qi¹, and Ming Liu^{1,2,†}

Abstract—Curb detection is an important function in intelligent driving and can be used to determine drivable areas of the road. However, curbs are difficult to detect due to the complex road environment. This paper introduces CurbNet, a novel framework for curb detection, leveraging point cloud segmentation. Addressing the dearth of comprehensive curb datasets and the absence of 3D annotations, we have developed the 3D-Curb dataset, encompassing 7,100 frames, which represents the largest and most categorically diverse collection of curb point clouds currently available. Recognizing that curbs are primarily characterized by height variations, our approach harnesses spatially-rich 3D point clouds for training. To tackle the challenges presented by the uneven distribution of curb features on the xy-plane and their reliance on z-axis high-frequency features, we introduce the multi-scale and channel attention (MSCA) module, a bespoke solution designed to optimize detection performance. Moreover, we propose an adaptive weighted loss function group, specifically formulated to counteract the imbalance in the distribution of curb point clouds relative to other categories. Our extensive experimentation on 2 major datasets has yielded results that surpass existing benchmarks set by leading curb detection and point cloud segmentation models. By integrating multi-clustering and curve fitting techniques in our post-processing stage, we have substantially reduced noise in curb detection, thereby enhancing precision to 0.8744. Notably, CurbNet has achieved an exceptional average metrics of over 0.95 at a tolerance of just 0.15m, thereby establishing a new benchmark. Furthermore, corroborative real-world experiments and dataset analyzes mutually validate each other, solidifying CurbNet’s superior detection proficiency and its robust generalizability. The code and dataset will be open sourced to: <https://github.com/guoyangzhao/CurbNet/>.

Index Terms—Point cloud, Curb detection, Segmentation, Deep learning, Autonomous driving.

I. INTRODUCTION

Autonomous vehicles fundamentally depend on analyzing data from onboard sensors to understand their surrounding environment, a cornerstone for safe driving [1], [2]. In this context, road boundary detection is a crucial aspect of perception, delineating road and non-road areas [3]. This distinction is vital for the positioning, planning, and decision-making of self-driving cars, especially under conditions where GPS signals are obscured by trees and buildings. In such urban road environments, curbs serve as a key and effective feature for vehicle localization [4], [5]. Despite their importance, curbs, typically linear, thin, and long, pose a significant challenge for detection in complex road environments [6].

Manuscript received April 19, 2021; † corresponding author.

¹G. Zhao, F. Ma, W. Qi and M. Liu are with the Robotics and Autonomous Systems Thrust, The Hong Kong University of Science and Technology (Guangzhou), Guangzhou, China.

²Y. Liu is with The Hong Kong University of Science and Technology, Hong Kong SAR, China

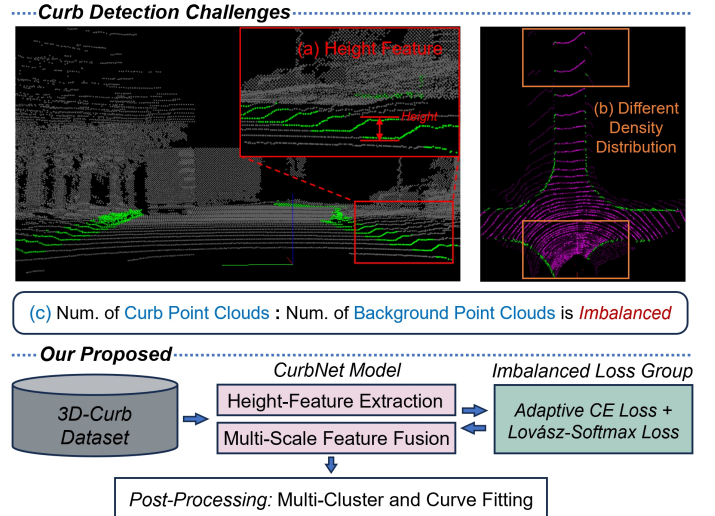


Fig. 1. Curb detection challenges and our proposed method. Three main challenges of curb detection are shown (a) height feature extraction (b) different density distribution of point clouds (c) Curb point cloud quantity proportion imbalance. Solution: First propose a 3D-Curb dataset. The MSCA module is designed to extract features of the xy, xz and yz planes and perform multi-feature fusion. The loss group is proposed to solve the imbalance problem. Finally, we use post-processing to further improve performance

Research in curb detection varies based on sensor technology, broadly categorized into vision-based and LiDAR-based methods [7]. This includes the use of monocular cameras, stereo vision, and combinations of 2D and 3D LiDAR sensors. Vision-based methods can provide rich contextual information and achieve effective detection results. However, camera performance is greatly influenced by light and weather conditions and fails to provide accurate depth information directly, which is a critical need for autonomous driving applications [8], [9]. Furthermore, the subtle color differences between regular road surfaces and curbs make it difficult for cameras to accurately detect curbs. In contrast, LiDAR sensors demonstrate robustness under various weather and lighting conditions and offer precise distance measurements [10]. Recently, 3D LiDAR has become one of the most important sensors for perceiving 3D environments in autonomous vehicles [11], [12].

Curb detection using LiDAR can be classified into manual feature methods and learning based methods [13]. Manual design feature methods [14], [15] typically analyze geometric relationships such as height and angle changes between adjacent points, given the difference between drivable roads and curbs [16], [17]. Most curb detection methods follow a sequential point cloud processing procedure [18], [19], including stages of candidate region extraction, manual feature setting and clustering, and post-processing for fitting estimation. These

methods, due to their interpretability in terms of safety, are widely used in curb detection for autonomous driving systems. However, the reliability of these manually designed rule-based processes is limited in practical applications, as errors in early detection stages can severely impact subsequent recognition performance. Additionally, they heavily rely on manual feature design, necessitating extensive parameter adjustments for various scenarios such as straight roads, curved roads, and different types of intersections, resulting in low practical efficiency and generalization [16], [20].

As deep learning has made breakthrough applications in perception, its capabilities in automatic feature extraction and learning have significantly reduced the tedium of manual feature design and parameter adjustment [21]. Particularly, in addressing different road scenarios, it has substantially enhanced model recognition performance and robustness [22]. Recently, some researchers have explored curb detection using CNN-based methods, projecting 3D LiDAR point cloud data into 2D images from a Bird's Eye View (BEV) perspective, followed by processing these images with CNN models to detect curbs [23], [24]. However, this direct projection of 3D LiDAR data can lead to the loss of essential spatial structural information, particularly the crucial height difference information for curb detection [25].

Considering current research in curb detection and the physical properties of 3D LiDAR, we have identified several challenges that need addressing, as shown in Fig. 1: (a) The primary distinguishing feature of curbs is the subtle height variation from the road surface [14], a challenging feature for models to accurately learn. (b) Curb point clouds from LiDAR scanning show significant distribution differences across various distances [26]. (c) Curbs occupy only a small portion of LiDAR point clouds, appearing as long and narrow lines, making effective model training difficult [25].

We first propose the 3D-Curb dataset, which contains up to 7100 frames of 3D annotated point cloud data, covering a wide range of road scenes. Unlike most existing algorithms that project 3D point clouds onto 2D images, we extract features directly from 3D point clouds, preserving crucial 3D spatial information. For the challenge (a) and (b), we draw inspiration from the cylindrical voxelization approach [27], aligning the model's input data more closely with the physical distribution of LiDAR scans. We then propose a multi-scale and multi-channel attention module, focusing not only on changes in the Z-axis height but also on enhancing the performance of multi-scale feature fusion. For the challenge (c), the difficulty of curb training in autonomous driving is objectively caused by the sparse quantity of curb point clouds. Categories related to curbs (like roads and sidewalks) can assist in the model's detection of curbs. Addressing the severe imbalance in point cloud quantities among different categories, we introduce a new loss combination, including a adaptive cross-entropy loss and an IoU-focused loss. Finally, in order to further improve the precision of curb detection, we proposed a post-processing scheme of multi-cluster and then fitting, which effectively removes the noise around the curb detection results.

Our primary contributions are summarized as follows:

1) Introducing a comprehensive 3D-Curb point cloud

dataset, to our knowledge which is the largest and most diverse currently available.

- 2) Proposing a new multi-scale and channel attention module and an imbalance loss strategy, based on the distribution characteristics of curb point clouds.
- 3) Implementing a multi-cluster fitting post-processing approach to further enhance detection performance.
- 4) Achieving state-of-the-art detection results in complex, large-scale intersection scenarios.

II. RELATED WORKS

A. Manual Feature Extraction Methods

In the early development of LiDAR technology, researchers designed mathematical functions to manually extract curb features by understanding the principles of LiDAR scanning. This process primarily involves stages of feature point extraction, feature point classification and filtering, and curb curve fitting and estimation. In [28], feature points are extracted through image segmentation and energy minimization, followed by the application of principal curves and surfaces methods in [29] for fitting detected curbs. Studies like [14], [15], [30], [31] utilize the horizontal and vertical continuity of point clouds, employing angle and height thresholds for curb feature extraction and using Gaussian Process Regression (GPR) and Random Sample Consensus for curb curve fitting. [15], [16] integrate the generalized curvature method from LOAM [23] into curb detection, refining the process with Gaussian Process Regression. [16], [32] detect curbs by analyzing ring compression in dense 3D LIDAR data, employing false positive filters and least-squares regression filters based on height values, respectively. [19], [33] propose sliding-beam segmentation and sliding-window detection methods by analyzing individual LiDAR scan lines, focusing on specific curb detection in each frame.

However, these manual feature extraction and sequential processing methods are inefficient. Not only is feature creation laborious and requires specialized knowledge, but early-stage erroneous selections can impact later detection phases, making them inadequate for complex road scenes and diverse curb shapes as noted in [34]. In this context, the advent of deep learning methods effectively solved the issues of feature extraction and generalization.

B. Deep Learning Methods

With the advancement of deep learning, some researchers have begun using CNNs to detect curbs in LiDAR point clouds, achieving notable performance. A common characteristic of deep learning-based curb detection methods is the transformation of input 3D point cloud data into 2D view images or voxelization. [35] uses camera images, LiDAR, and elevation gradients of LiDAR as inputs, employing convolutional recurrent networks to extract road boundaries in 2D BEV images to construct semantic maps. [24] projects motion-accumulated 3D point cloud data onto 2D BEV images, initially detecting visible road edges through a U-Net network [36], followed by predicting obscured road boundaries using multi-layer convolutional networks with expanded receptive

fields [37]. Similarly, [23] proposes a two-stage curb detection framework, initially employing U-Net for visible curb detection, then incorporating uncertainty quantification to improve detection performance in obscured areas.

Compared to traditional methods, these approaches demonstrate robustness in various driving environments and reduce the burden of manual parameter tuning. However, converting point clouds to 2D images results in significant loss of 3D information, especially the height difference features crucial for distinguishing curbs from other categories. [38] explores voxelizing the raw 3D point cloud as a superimage input to the model, using CNNs to detect road edges and lane markings. However, 3D model recognition accuracy remains low. LCDeT [25] employs a Transformer model for curb detection in voxelized point clouds, introducing dual attention mechanisms in both temporal and spatial dimensions to ensure detection stability and accuracy. Yet, this method relies on complex model structures and high-resolution LiDAR sensors.

Our proposed method uses a single, original 3D point cloud as input, preserving more 3D feature information. Addressing the uneven distribution of LiDAR features in curb recognition scenes and the easy loss of curb height difference information, we introduce multi-scale and multi-channel attention mechanisms to enhance model recognition performance.

C. Curb Detection Datasets

There is a significant amount of research in LiDAR-based curb detection; however, high-quality datasets with curb annotations are scarce. Major automotive datasets such as NuScenes [39], KITTI [40], and SemanticKITTI [41] do not include curb annotations. The robustness of deep learning methods is closely related to the volume of data collected under various environmental conditions. These factors have somewhat hindered the application of deep learning methods in this task. [19] created a public dataset for curb detection, comprising 200 scans collected across five different scenes. [23] developed a public dataset for curb detection, including 5200 scans with Bird’s Eye View (BEV) labels, collected from urban areas. LCDeT [25] introduced a curb dataset for 128-beam LiDAR, containing 6200 frames of point clouds from urban road scenes, both during daytime and nighttime. [26] proposed a method for 3D curb detection and annotation in LiDAR point clouds, effectively reducing manual annotation time by 50%.

The above-mentioned curb point cloud datasets only label the curb category, which cannot be directly used in autonomous driving scenarios, as recognition of other categories such as vehicles and roads is also necessary. Similarly, other categories surrounding the curb, like roads and sidewalks, can also assist the model in more accurately learning curb features. Based on the existing large SemanticKITTI dataset, we added annotations for the curb category, thereby covering a richer array of real road scenes, totaling up to 7100 frames of point cloud data. To our knowledge, this is currently the largest and most comprehensive curb point cloud dataset with annotations relevant to autonomous vehicles (AV). Table. I illustrates the related LiDAR datasets for curb detection.

TABLE I
COMPARISON OF RELATED CURB DATASETS.

Dataset	LiDAR	Public	Frames	3D labeling	Categories
Zhang [19]	32-line	Yes	200	No	1
Liang [35]	-	No	-	No	1
Suleymanov [24]	-	No	-	No	1
Uncertainty [23]	32-line	Yes	5224	No	2
NRS [25]	128-line	Yes	6220	No	2
3D-Curb (ours)	64-line	Yes	7100	Yes	29

III. METHODOLOGY

A. 3D-Curb Dataset Construction

Compared to other scenarios in autonomous driving, there is a notable lack of relevant curb point cloud datasets, especially those annotated for 3D point clouds. We have developed and proposed the 3D-Curb dataset based on the large-scale, open-source SemanticKITTI dataset [41], adding a new curb category while retaining the other original 28 semantic categories. This dataset was collected using a 64-line LiDAR, providing a comprehensive view of various street scenes as a universal autonomous driving dataset. In the dataset creation process, we adopted the method proposed by [34] to initially extract curb locations in a Bird’s Eye View (BEV) perspective, followed by manual annotation of representative scenes in 3D point cloud data. The 3D-Curb dataset focuses on curb annotations in the forward direction of vehicle travel, with an average range of 40.43 meters along the forward y-axis. To accentuate the curb areas, the lateral x-axis range is set to 1.3 times the road width.

The 3D-Curb dataset encompasses all scenes from sequences 00-10 in the SemanticKITTI dataset, totaling 7100 frames of finely annotated curb point cloud data. To our knowledge, this is the largest curb point cloud dataset to date and the only one annotated in 3D. Table 1 presents a comparison with other relevant curb datasets.

B. Overview of Model Framework

As shown in Fig. 2, the CurbNet framework primarily consists of three parts: data voxelization, feature extraction, and feature decomposition and segmentation.

In the data voxelization section, to better align the input data structure to the physical characteristics of LiDAR point clouds (where the density of the circularly scanned point clouds decreases with increasing distance), we adopted a cylindrical partitioning format for point cloud voxelization, inspired by Cylinder3D [27]. We converted the Cartesian coordinates (x, y, z) of the point cloud into polar coordinates (radius ρ and azimuth angle θ), aligning more accurately with the scanning pattern of LiDAR and preserving the point cloud’s geometric structure to the greatest extent. The voxel division was then performed uniformly across the ρ , θ , and z dimensions, ensuring larger voxels for greater distances to minimize the impact of varying point cloud densities on feature learning.

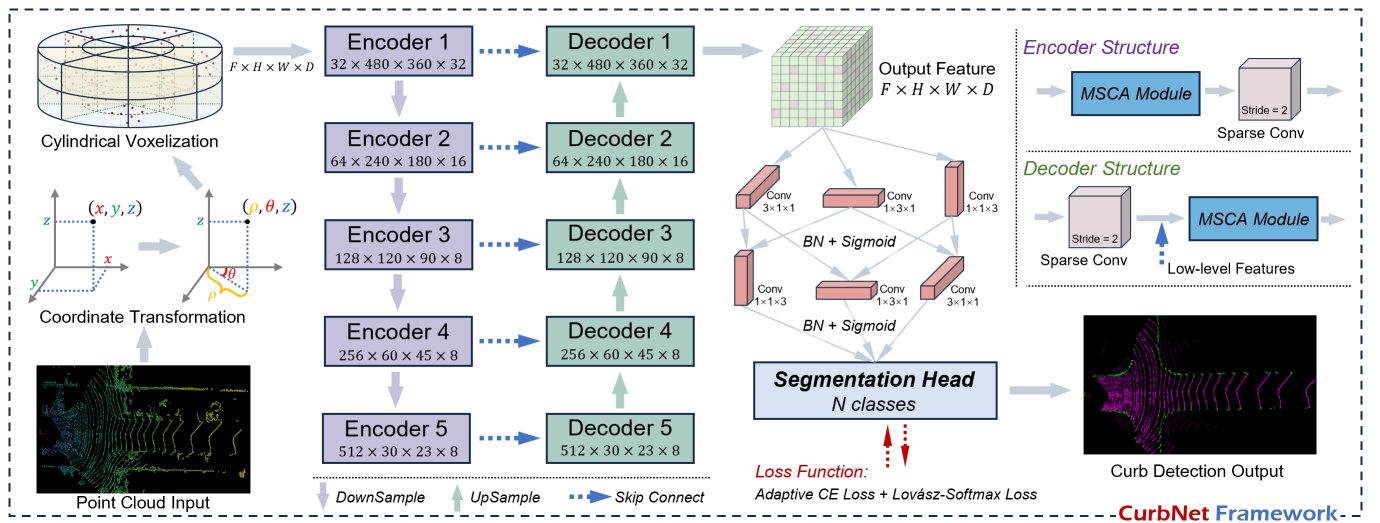


Fig. 2. **Overview of proposed CurbNet framework.** From left to right, first is the input data coordinate transformation and cylindrical voxelization. Then there is the U-Net shaped encoder-decoder structure. This is followed by feature decomposition and segmentation head. Finally, the model calculates loss and outputs detection results.

In the feature extraction stage, the voxelized features of dimensions $F \times H \times W \times D$ were fed into an end-to-end 3D U-Net model. Diverging from the classic U-Net model’s Encoder and Decoder structure, we proposed a Multi Scale and Channel Attention Module (MSCA) tailored to the characteristic distribution of curb point clouds, employing stride=2 Sparse Convolution for pooling functions.

In the feature decomposition and segmentation stage, we decomposed the output high-dimensional features of $F \times H \times W \times D$. After the training, the feature tensor is high-rank [42], and its rich context encoding information incurs substantial modeling costs in the point cloud segmentation process. Inspired by high-rank matrix decomposition theory [43], we performed low-rank decomposition on the $H \times W \times D$ dimensions using three one-dimensional convolution kernels: $3 \times 1 \times 1$, $1 \times 3 \times 1$, and $1 \times 1 \times 3$, respectively. We use two layers of low-rank decomposition and add dense connections to thereby increase feature aggregation and provide more reference features for the segmentation head. The weights for each dimension were modulated through the Sigmoid function. Finally, context features were aggregated to consolidate features and output segmentation results efficiently.

C. Multi Scale and Channel Attention (MSCA) Module

The structure of the MSCA as shown in Fig. 3, constitutes a fundamental component of both the Encoder and Decoder. Curb point clouds typically form a long curve along both sides of the road, but with the increasing scanning distance of LiDAR, the point cloud density decreases, leading to sparser curb point cloud features. This results in significant scale differences in the features represented by the same number of point clouds at different distances after voxelization. Drawing on multi-feature fusion methods [44], we uniformly blend multi-scale features derived from different convolutional kernel outputs.

The primary distinguishing features of curbs lie in the subtle height differences between the road and sidewalks, i.e., the differences along the Z-axis in the point cloud features. Unlike the Cylinder3D [27] general point cloud segmentation

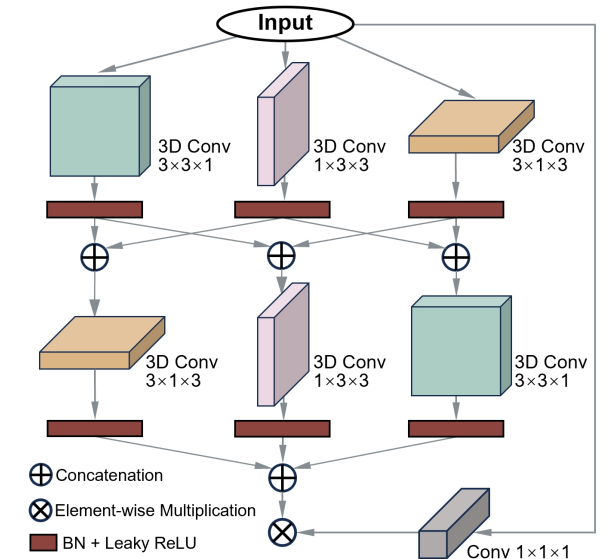


Fig. 3. **Structure of multi-scale and channel attention (MSCA) module.** Three convolutions are used to match the target area on the spatial xy , xz and yz planes, and dense connections are used to obtain the multi-scale features of the curb.

algorithm, which only focuses on feature learning in the xy plane and overlooks curb’s high-frequency feature information on the Z-axis, we have added a convolution module for the Z-axis D dimension. This module makes the model more attuned to curb’s high-frequency features in height differences. Inspired by text detection methods [26], we employed three asymmetrical convolution kernels to match the target areas in the xy , xz , and yz planes of the space, thereby capturing the curb feature information. Compared to the structure of two traditional $3 \times 3 \times 3$ convolutions chained together, the MSCA module (Fig. 3) achieves thrice the efficiency in feature extraction and blending, with the same receptive field and computational resource consumption.

D. Loss Group

In the context of curb detection for autonomous driving, we propose a novel combination of loss functions to adapt to

the class imbalance in training data. In real-world scenarios, the point cloud data for curbs comprises only a small fraction compared to other categories such as roads and buildings. Using uniform loss weights can lead to training imbalances, adversely affecting the recognition performance for the minority class, i.e., curbs. To address this, we introduce a combination of Adaptive Cross-Entropy (CE) Loss and Lovász-Softmax Loss.

1) Adaptive CE Loss

This paper improves upon the standard Cross-Entropy (CE) Loss by adjusting weights based on the distribution of point cloud data across different classes, enabling the model to focus more on learning from scarce sample data. The standard CE Loss is defined as:

$$\mathcal{L}_{CE} = -y_1 * \log(p_1) - y_2 * \log(p_2) \quad (1)$$

where y_i represents the true label and p_i represents the predicted probability for class i .

To address class imbalance, we modify the loss weights for different classes using the α parameter, akin to the weighted CE Loss. In this context, α is computed based on the inverse ratio of point cloud quantities of each class, followed by normalization. The formulation of the Weighted CE Loss (\mathcal{L}_{WCE}) is:

$$\mathcal{L}_{WCE} = -\alpha_1 * y_1 * \log(p_1) - \alpha_2 * y_2 * \log(p_2) \quad (2)$$

where α_i is the class-specific weight calculated as:

$$\alpha_i = \frac{1}{\log(\delta + \frac{N}{N_i})} \quad (3)$$

Here, N is the total number of points in the point cloud, N_i is the number of points in class i , and δ is a small constant to prevent division by zero.

Further drawing inspiration from Focal Loss, we introduce a modulation factor $(1 - P_i)^\gamma$ into the cross-entropy loss, effectively reducing the weights for easily classified samples and increasing them for the more challenging ones, thereby directing the training focus towards difficult-to-classify samples. The Adaptive CE Loss (\mathcal{L}_{ACE}) is therefore formulated as:

$$\begin{aligned} \mathcal{L}_{ACE} = & -\alpha_1 * (1 - p_1)^\gamma * y_1 * \log(p_1) \\ & - \alpha_2 * (1 - p_2)^\gamma * y_2 * \log(p_2) \end{aligned} \quad (4)$$

The focusing parameter γ , which modulates the emphasis on difficult samples, is set to 2 in this study.

2) Lovász-Softmax Loss

Lovász Loss is particularly effective in handling imbalanced datasets and excels in addressing sparse boundary issues [45]. Compared to traditional cross-entropy loss, it demonstrates superior performance in terms of Intersection over Union (IoU) scores, commonly used for evaluating image segmentation results due to their quality perception and scale invariance. In Lovász Loss, for a given true label vector \mathbf{y}^* and a predicted label vector $\tilde{\mathbf{y}}$, the IoU index for class c is defined as:

$$\text{IoU}_c(\mathbf{y}^*, \tilde{\mathbf{y}}) = \frac{|\{\mathbf{y}^* = c\} \cap \{\tilde{\mathbf{y}} = c\}|}{|\{\mathbf{y}^* = c\} \cup \{\tilde{\mathbf{y}} = c\}|} \quad (5)$$

This index provides the ratio between the intersection and union of the true and predicted masks within the range $[0, 1]$, with the convention $0/0 = 1$. The corresponding loss function employed in empirical risk minimization is:

$$\Delta_{\text{IoU}_c}(\mathbf{y}^*, \tilde{\mathbf{y}}) = 1 - \text{IoU}_c(\mathbf{y}^*, \tilde{\mathbf{y}}) \quad (6)$$

For multi-label datasets, it is customary to average across classes, yielding the Mean IoU (mIoU).

The Lovász-Softmax loss extends this concept by applying the Lovász extension to the softmax probabilities of a model's output. It optimizes a convex surrogate of the IoU score, which is more suitable for gradient-based optimization. Specifically, the Lovász-Softmax loss \mathcal{L}_{IoU} for a set of classes C is defined as:

$$\mathcal{L}(\mathbf{y}^*, \tilde{\mathbf{y}}) = \sum_{c \in C} \Delta_{\text{IoU}_c}(\mathbf{y}^*, \tilde{\mathbf{y}}) \quad (7)$$

The computation involves ordering the pixels by their error margin and computing a weighted sum of the individual errors, thus directly targeting the errors that most impact the IoU score.

In practice, the Lovász-Softmax loss is particularly beneficial for segmenting objects with irregular or sparse boundaries, as it focuses on the segments of the predictions that have the largest impact on the overall IoU score, rather than treating all errors equally.

E. Multi-Cluster and Curve Fitting

This paper introduces a post-processing method based on multi-cluster refitting to filter noise points from LiDAR data segmentation results, thereby enhancing the detection accuracy of curbs. Due to the increasing sparsity of LiDAR point clouds with distance and the potential interruption of curb lines due to obstructions, direct curb clustering along the sides of roads is challenging, as shown in Fig. 4. Thus, we adopt a multi-cluster strategy, treating the curb in multiple segments.

To address this challenge, we initially apply the Density-Based Spatial Clustering of Applications with Noise (DBSCAN) algorithm [46] for preliminary segmentation of the detected curbs. DBSCAN is characterized by its ability to identify clusters of arbitrary shapes without a predefined number of clusters, efficiently handling noise points. The core idea of DBSCAN revolves around setting a neighborhood radius ε (eps) and a minimum sample number minPts (min-samples) to determine cluster membership. In our study, we set eps to 1 and min-samples to 5.

Let P be a point in the point cloud; its ε -neighborhood, denoted as $N_\varepsilon(P)$, is defined as:

$$N_\varepsilon(P) = \{Q \in \text{Dataset} \mid \text{dist}(P, Q) \leq \varepsilon\} \quad (8)$$

where $\text{dist}(P, Q)$ represents the distance between points P and Q . A point P is considered a core point if its ε -neighborhood contains at least minPts points, i.e., $|N_\varepsilon(P)| \geq \text{minPts}$.

Post-clustering, we fit polynomial curves to each independent curb segment. The key is to precisely fit the geometric shape of the curb while eliminating noise points not belonging

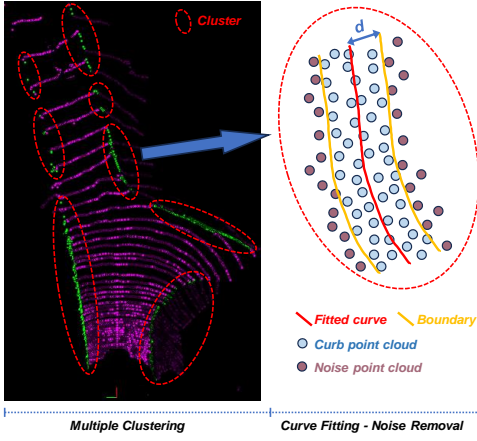


Fig. 4. **Process of multiple clustering and fitting to remove noise points.** The left figure shows the effect of multiple clustering in discontinuous scenes. The right figure shows the method of curve fitting and setting distance to remove noise points.

to the curb. After polynomial curve fitting of each segment, by calculating the distance from points to the fitted curve, we can effectively identify and eliminate noise points located outside the fitted curve, as shown in Fig. 4.

During the polynomial curve fitting of curbs, the aim is to eliminate noise points not belonging to the curb. Assuming the curve equation is $f(x)$, for any point $P(x, y)$ in the point cloud, we calculate the perpendicular distance d from the point to the curve:

$$d(P, f) = |y - f(x)| \quad (9)$$

If $d(P, f)$ exceeds a predetermined threshold δ , the point P is considered noise and is removed from the dataset:

$$\text{If } d(P, f) > \delta, \text{ then } P \text{ is noise} \quad (10)$$

The complete operation process is shown in Algorithm 1. Through this approach, combining the DBSCAN algorithm with polynomial curve fitting effectively identifies and extracts accurate curb lines from LiDAR point cloud data, while eliminating noise points, thus improving the overall segmentation accuracy.

IV. EXPERIMENT AND ANALYSIS

A. Experiment Setup

1) Training Details

Our model training was conducted in an Ubuntu 20.04 environment, utilizing an Intel(R) Xeon(R) Gold 5318S CPU @ 2.10GHz and an NVIDIA RTX 3090 GPU. We employed the PyTorch framework for model training, using the Adam optimizer. The training parameters were set with a batch size of 8 and a total of 100 epochs, at a learning rate of 0.001.

Regarding the datasets, we employed two distinct datasets for training and evaluation: the publicly available NRS dataset and our custom-built 3D-Curb dataset. Both datasets comprised curb data collected from forward-facing trajectories, each extending over 40 meters. To enhance feature learning for curb detection, we augmented the training process by including two additional categories: road and sidewalk.

2) Evaluation Metrics

Algorithm 1 Multi-Cluster and Curve Fitting Post-Processing

Require: Point cloud data, ϵ , minPts, δ

Ensure: Refined curb line segmentation

- 1: **Step 1:** Apply DBSCAN to point cloud data
- 2: **for** each point P in point cloud **do**
- 3: Compute $N_\epsilon(P)$
- 4: **if** $|N_\epsilon(P)| \geq \text{minPts}$ **then**
- 5: Mark P as a core point
- 6: **end if**
- 7: **end for**
- 8: **Step 2:** Segment curb lines into clusters
- 9: **Step 3:** Fit polynomial curves to each curb segment
- 10: **for** each curb segment **do**
- 11: Fit polynomial curve $f(x)$
- 12: **for** each point $P(x, y)$ in segment **do**
- 13: Calculate perpendicular distance $d(P, f)$
- 14: **if** $d(P, f) > \delta$ **then**
- 15: Remove P as noise
- 16: **end if**
- 17: **end for**
- 18: **end for**
- 19: **Step 4:** Output refined curb line segments

The performance of our curb detection method was rigorously evaluated using standard metrics. These include Precision, Recall, and F-1 score, which are quintessential for quantifying the accuracy and reliability of classification models. Precision, defined as $\frac{TP}{TP+FP}$, measures the proportion of correctly predicted positive observations to the total predicted positives. Recall, calculated as $\frac{TP}{TP+FN}$, assesses the proportion of actual positives that were correctly identified. The F-1 score, given by $2 \times \frac{\text{Precision} \times \text{Recall}}{\text{Precision} + \text{Recall}}$, harmonizes the balance between Precision and Recall, providing a single measure of efficacy. Here, TP (True Positives) represents the number of correct positive predictions, FP (False Positives) denotes the count of negative instances incorrectly classified as positive, TN (True Negatives) refers to the count of correct negative predictions, and FN (False Negatives) signifies the instances where positive cases were wrongly predicted as negative. These metrics collectively offer a comprehensive view of our model's performance, crucial for its validation in high-level applications.

B. Quantitative Results of Curb Detection

1) Model Training Results

In the NRS dataset experiments (refer to Table. II), this study compared classic segmentation algorithms such as PointPillars, U-Net, Swin-Transformer, and CSWin-Transformer, as well as the state-of-the-art curb detection model, LCDeT. Thanks to the specially designed MSCA module for Curb 3D scenarios, our proposed CurbNet achieved the highest detection performance on the NRS dataset, with Precision, Recall, and F-1 scores reaching 0.8280, 0.8341, and 0.8309, respectively.

The experiments in the 3D-Curb dataset not only compared classic and advanced deep learning model algorithms but

TABLE II
COMPARISON OF RESULTS IN NRS-DATASET [25].

Method	Precision	Recall	F-1 score
PointPillars [47]	0.759	0.6019	0.6524
U-Net [36]	0.7546	0.7018	0.7172
Swin-T [48]	0.7216	0.7034	0.7001
CSWin-T [49]	0.7692	0.6597	0.6966
LCDeT [25]	0.8257	0.8050	0.8092
CurbNet (ours)	0.8280	0.8341	0.8309
CurbNet-post (ours)	0.8420	0.8497	0.8458

TABLE III
COMPARISON OF RESULTS IN 3D-CURB DATASET.

Difference	Methods	Precision	Recall	F-1 score
Manual feature	Zhang [19]	0.6854	0.6564	0.6053
	Sun [9]	0.6878	0.6864	0.6297
	Wang [14]	0.7209	0.7013	0.6973
Deep Learning	3D U-Net [50]	0.7695	0.7492	0.7592
	Cylinder 3D [27]	0.8049	0.8038	0.7942
	CurbNet (ours)	0.8293	0.8569	0.8429
	CurbNet-post (ours)	0.8744	0.8648	0.8696

also included three traditional methods of manual feature extraction, as shown in Table. III. Owing to the robust automatic feature extraction capabilities, deep learning methods significantly outperformed in curb detection, surpassing the other methods by over 10 points in Precision, Recall, and F-1 score. Among the deep learning methods, our CurbNet surpassed the best-performing supervised learning model on the SemantickITTI dataset, Cylinder3D, by more than 2 points in Precision. This demonstrates the exceptional performance of CurbNet in the field of curb point cloud segmentation.

2) Tolerance Results

Since curbs resemble elongated curves, relevant research often further tests model performance within a certain error range. Experiments are typically conducted in meters and pixels, with 1 pixel approximately equal to 0.1m of Tolerance, and common experimental settings range from 0.1m to 0.4m.

In our study, we conducted Tolerance performance tests on the 3D-Curb dataset, setting four Tolerances ranging from just 0.05m to 0.2m, as shown in Table. IV. Tests were carried out on three models: 3D U-Net, Cylinder 3D, and CurbNet (ours). With the increase in error Tolerance, performance metrics improved significantly. At 0.05m Tolerance, Precision improved by an average of 4 points; at 0.1m, by 9 points; at 0.15m, by 12 points; and at 0.2m, by 13 points. As Tolerance increased, performance gains gradually reached saturation. Notably, our CurbNet exceeded 0.95 in the average values of Precision, Recall, and F-1 score at just 0.15m Tolerance. This represents the optimal performance achieved in curb detection based on point cloud segmentation.

C. Visualization Results of Curb Detection

We conducted a visual analysis of the test results obtained using our CurbNet model, comparing them with the ground

truth to further validate the model’s detection performance. Fig. 5 illustrates the visualization results in scenarios without obstructions, showcasing the curb detection results in five common road scenes: straight road, curved road, right-angle intersection, curved intersection, and cross intersection. The images clearly demonstrate that the CurbNet model successfully identified all curb lines present in the ground truth, even in complex intersection scenarios. Notably, in the curved intersection scenario, the results identified by CurbNet were even more precise than the ground truth annotations, showcasing our model’s exceptional feature extraction capabilities and generalizability.

Fig. 6 also displays the visual recognition results in scenarios with obstructions, where yellow dashed circles highlight the obstructed areas. Despite the absence of point clouds in obstructed areas, the model accurately identified curbs in the other parts without being influenced by the obstructed regions. As long as the input data contained curb features, CurbNet could accurately detect them, unaffected by the obscured areas.

Furthermore, we conducted a visual analysis of the results on the NRS dataset, as shown in Fig. 7. This analysis primarily showcases curb detection in five common road scenarios and four special intersection types. Through a comparative visualization of the detection results and ground truth, our proposed CurbNet accurately identified the respective curb features.

D. Post-Processing Experiment

In this paper, we conducted controlled experiments to compare the proposed post-processing method. Given the use of multiple clustering followed by curve fitting in post-processing, the setting of clustering parameters plays a crucial role in its effectiveness. Based on the road width and point cloud density characteristics of the 3D-Curb dataset, we experimented with varying the distance variable Eps (from 1m to 4m) and the minimum sample points variable minPts (from 2 to 200), as illustrated in Fig. 8.

As the clustering distance Eps increases, changes in the performance metrics of post-processing become more gradual and similar. However, when the minimum sample points minPts are lower, the performance decreases compared to when Eps is 1m. This is attributed to the larger curb clustering caused by greater clustering distances, resulting in minimal changes post-curve fitting. Additionally, larger clusters tend to overlook sparsely distributed point clouds during curve fitting, thereby reducing performance.

Fig. 8 clearly demonstrates that as the minimum sample points variable minPts increases, the Precision metric of post-processing gradually improves, but both Recall and F-1 score metrics significantly decrease, especially at Eps settings of 1m and 2m. This decline is due to the increase in the number of minPts leading to the neglect of sparsely distributed curb point clouds at greater distances, resulting in a noticeable drop in Recall and F-1 scores.

Based on comparative experimental results and trade-off between metrics, smaller Eps distances and fewer minPts numbers yield the most optimal post-processing outcomes.

TABLE IV
COMPARISON OF DIFFERENT TOLERANCES IN 3D-CURB DATASET.

Tolerance (m)	Precision				Recall				F-1 score			
	0.05	0.10	0.15	0.20	0.05	0.10	0.15	0.20	0.05	0.10	0.15	0.20
3D U-Net [50]	0.8293	0.8583	0.8881	0.9012	0.8078	0.8498	0.8745	0.8843	0.7933	0.8389	0.8662	0.8777
Cylinder 3D [27]	0.8403	0.8909	0.9221	0.9360	0.8588	0.9007	0.9253	0.9355	0.8391	0.8856	0.9136	0.9257
CurbNet (ours)	0.8665	0.9160	0.9460	0.9589	0.9031	0.9433	0.9664	0.9761	0.8844	0.9294	0.9561	0.9674
CurbNet-post (ours)	0.9139	0.9532	0.9682	0.9740	0.8974	0.9301	0.9439	0.9501	0.9056	0.9415	0.9559	0.9619

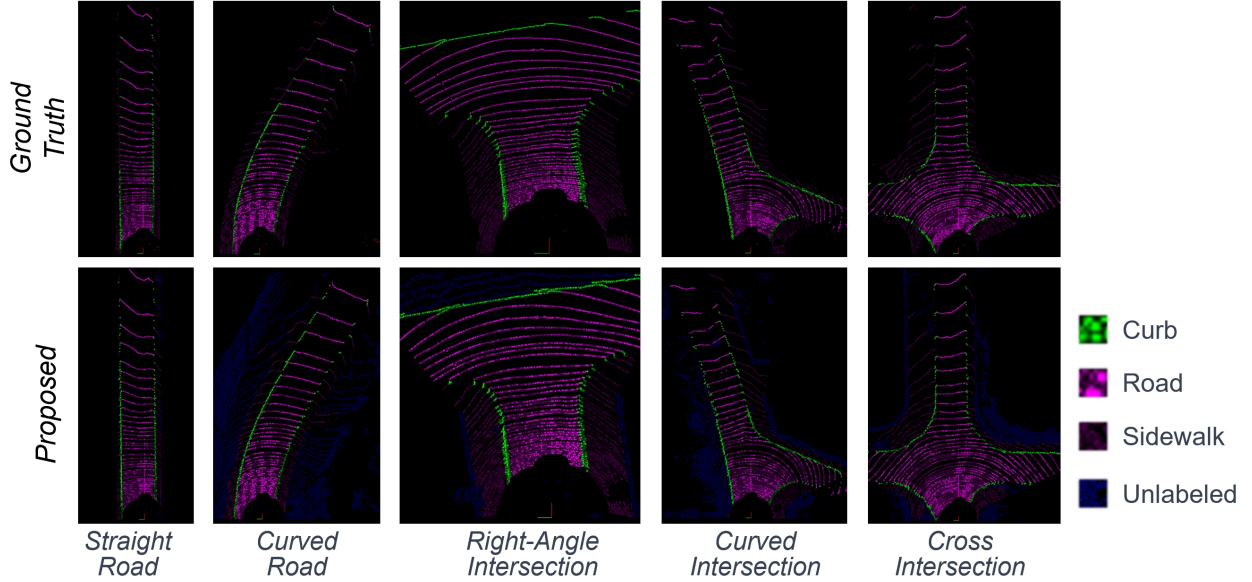


Fig. 5. Curb detection result in 3D-Curb dataset. We compared the curb detection results at five classic intersections. The model accurately detected the curb area and was even better than the ground truth on the curve road.

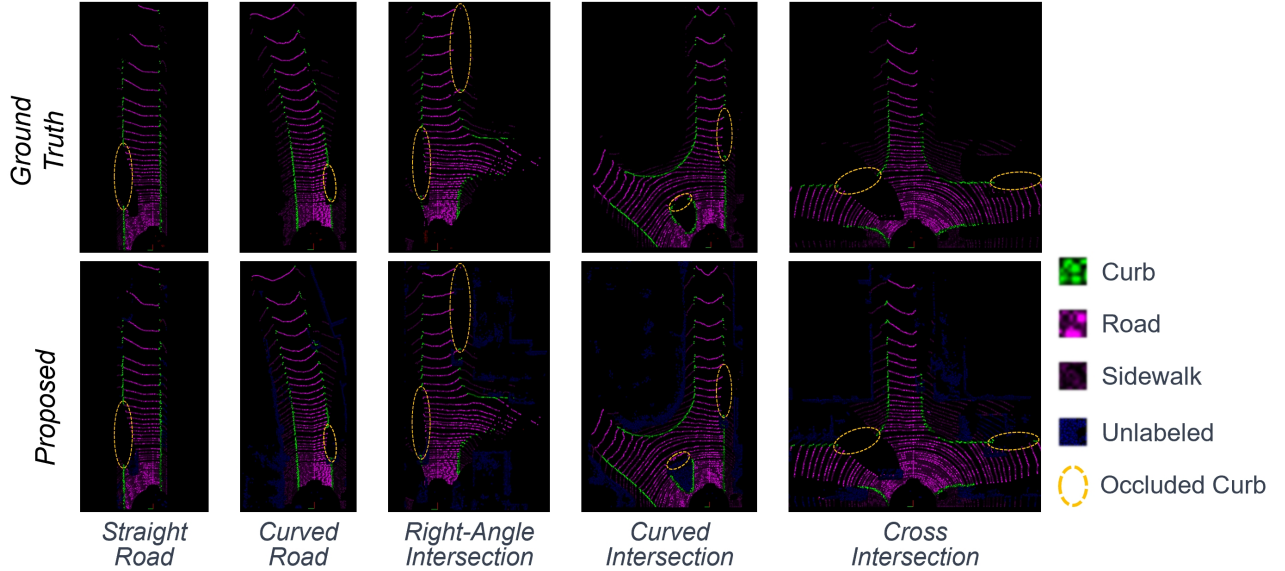


Fig. 6. Curb detection result in 3D-Curb dataset under occlusion. We compared the curb detection results at five classic intersections with occlusion. Even if there is occlusion, it does not affect the curb detection in other areas at all.

E. Ablation Study

As shown in Table. V, this study conducted comparative ablation experiments focusing on the main loss functions and crucial module designs of our model. We first conducted individual experiments on the employed \mathcal{L}_{CE} (Cross-Entropy), \mathcal{L}_{ACE} (Adaptive Cross-Entropy), and \mathcal{L}_{IoU} (Intersection over Union) losses. Subsequently, we tested combinations of $\mathcal{L}_{CE}+\mathcal{L}_{IoU}$ loss and $\mathcal{L}_{ACE}+\mathcal{L}_{IoU}$ loss. In the experimental

results, due to the design of the \mathcal{L}_{ACE} loss addressing the imbalance in the number of curb point clouds compared to other categories, its disproportionate weight settings caused the model to overly focus on recall during training. However, the interaction with the \mathcal{L}_{IoU} loss led to a more balanced overall performance, achieving optimal detection capabilities. The $\mathcal{L}_{ACE}+\mathcal{L}_{IoU}$ loss combination outperformed the $\mathcal{L}_{CE}+\mathcal{L}_{IoU}$ loss group by 1.5 points in Precision and 2 points in Recall.

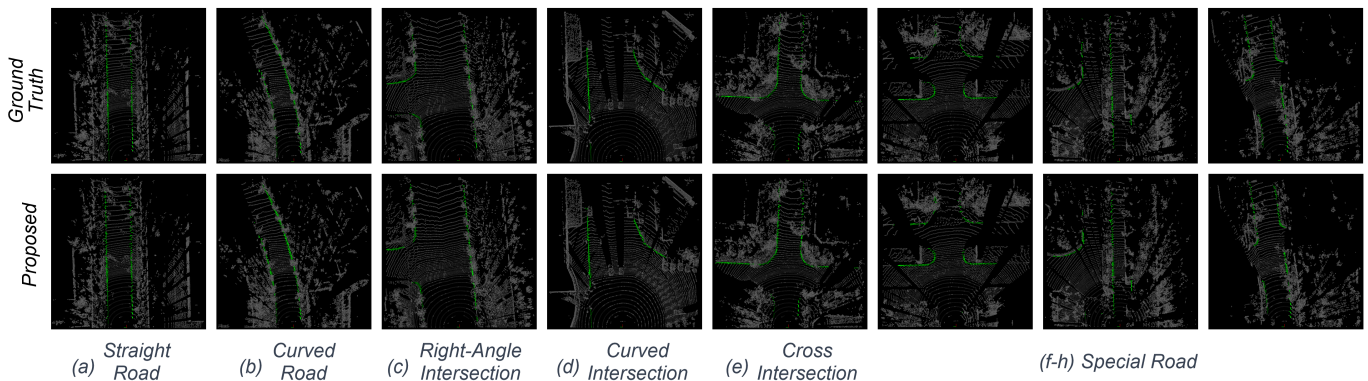


Fig. 7. Curb detection result in NRS Dataset. The excellent detection performance and generalization of the proposed method are well demonstrated on the NRS data set, and accurate detection can be performed even at the special intersection (f-h).

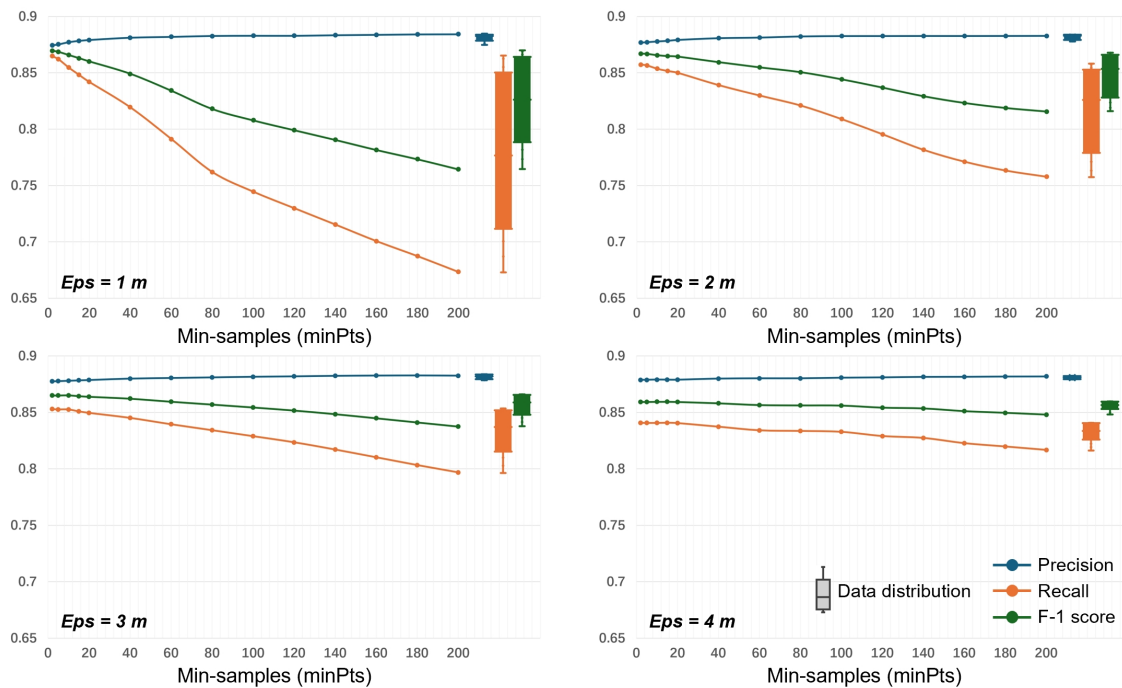


Fig. 8. Parameter adjustment experiments for multiple clustering and fitting. We conduct control variable experiments on the main parameter distance variable Eps and the minimum sample point variable minPts of DBSCAN clustering. The fewer minPts, the better the overall performance.

TABLE V
ABLATION OF DIFFERENT LOSS FUNCTIONS AND MODULES

\mathcal{L}_{CE}	\mathcal{L}_{ACE}	\mathcal{L}_{IoU}	MSCA	Precision	Recall	F-1 score
✓			✓	0.8174	0.8303	0.8238
	✓		✓	0.7833	0.8807	0.8290
		✓	✓	0.8234	0.8367	0.8339
✓		✓	✓	0.8186	0.8472	0.8374
	✓	✓		0.8297	0.8496	0.8395
	✓	✓	✓	0.8310	0.8698	0.8499

Finally, we compared the model’s performance with and without the MSCA module. Under the $\mathcal{L}_{ACE} + \mathcal{L}_{IoU}$ loss setting, including the MSCA module significantly enhanced the corresponding performance metrics, particularly increasing Recall by 2 points and F-1 score by 1 point.

F. Real Scene Experiment

To further validate the performance and effectiveness of the proposed method, we conducted real-world experiments in

addition to the dataset experiments. As depicted in Fig. 9, we utilized an autonomous delivery vehicle as our experimental platform, equipping it with a LiDAR sensor system mounted on its top. The LiDAR used was the OS1-U model with 128 beams, manufactured by Ouster. To ensure the generalizability of our experiments, the autonomous vehicle was driven on roads within the HKUST Guangzhou campus. Data collection and curb detection were carried out in five different road segments (Scene A, B, C, D, and E), as shown in the map in Fig. 9. These segments included both standard road scenarios (straight roads, bends, and intersections) and complex ones (roundabout turns and intricate junctions).

The curb detection results in the 5 scenes are illustrated in Fig. 10, where we selected 8 representative images from each scene for visual analysis. Overall, our method achieved commendable curb detection results in each scene, further demonstrating the robust curb feature extraction capability of the CurbNet model. In individual cases, our proposed method accurately detected not only the evident, extensive curbs, but also achieved remarkable results on small-scale curbs, which

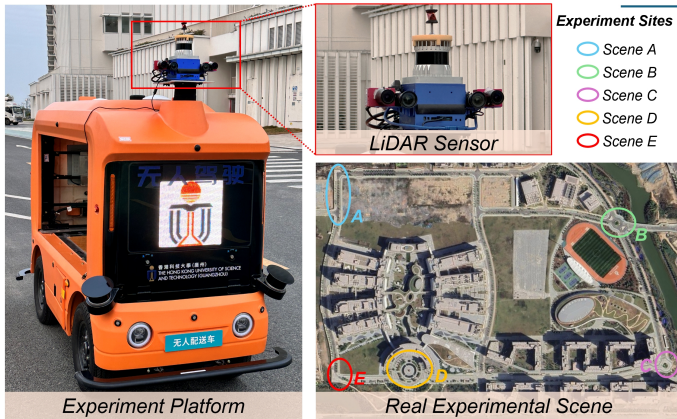


Fig. 9. **Setup of real scene experiment.** We used the delivery vehicle equipped with LiDAR to conduct real scene experiments. There are a total of five experimental sections distributed on the HKUST Guangzhou campus.

TABLE VI
RESULTS IN FIVE REAL SCENES.

Site	Precision	Recall	F-1 score
Scene A	0.8331	0.8821	0.8569
Scene B	0.8950	0.8123	0.8517
Scene C	0.8610	0.8366	0.8530
Scene D	0.8018	0.8533	0.8268
Scene E	0.8579	0.8388	0.8483
All Scene	0.8462	0.8443	0.8453

are typically less conspicuous and easily overlooked, as seen in Scene B (image d) and Scene D (images b and c). This success can be attributed to the model’s design focusing on multi-scale feature fusion and multi-channel feature extraction. Similarly, our method also exhibited superior detection performance in complex intersection scenarios with irregular curb distributions (Scene B and Scene C). Particularly in Scene B, the method precisely detected all curbs present in the LiDAR point cloud, a feat attributable to the powerful curb feature extraction ability of the MSCA module.

Finally, this paper also quantitatively evaluates the real scene experiments by testing key metrics, the results as shown in Table. VI. By comparing with manually annotated ground truth data, CurbNet achieved an average Precision, Recall, and F1 score of 0.8462, 0.8443, and 0.8453, respectively, across the five scenes. Among them, the Recall and F-1 score indicators obtained in Scene A are the highest, which are 0.8821 and 0.8569 respectively, and the Precision indicators obtained in Scene B are the highest 0.8950. These results corroborate with those obtained from dataset testing, further substantiating the excellent detection performance and generalizability of the CurbNet model.

V. LIMITATION

While the method presented in this paper demonstrates effective and accurate detection of curbs in road scenes, thus providing a basis for navigable area determination for autonomous driving, it currently has limitations in detecting curbs solely within the LiDAR point cloud. Due to factors such as the scanning angle, field of view, and obstructions inherent

to LiDAR technology, some road areas remain undetected in the point cloud, leading to an inability of the model to extract corresponding curb features. This necessitates future research involving more advanced sensors to minimize scanning blind spots. Additionally, the development of a model incorporating a curb prediction module that operates effectively in areas without scanning blind spots is essential to mitigate the impact of these blind spots on curb detection.

VI. CONCLUSION

In this paper, we established the 3D-Curb dataset, comprising 7,100 frames. To our knowledge, this is currently the largest and most diverse curb point cloud dataset with the most extensive range of annotated categories. Notably, this is also the first dataset to feature 3D point cloud annotations for curbs, which will significantly aid future related research. Within the CurbNet framework, we introduced the Multi-Scale and Channel Attention (MSCA) module, addressing the challenges of uneven distribution of curb features on the xy-plane and the reliance on high-frequency z-axis features. Additionally, we developed an adaptive weighted loss function group to resolve the imbalance in the number of curb point clouds relative to other categories. Extensive experiments on both the NRS and 3D-Curb datasets demonstrated that our approach outperforms the current leading curb detection and point cloud segmentation models. In tolerance experiments, CurbNet achieved over 0.95 average performance in Precision, Recall, and F-1 score metrics at just 0.15m tolerance, setting a new standard. Furthermore, our post-processing approach of multi-clustering and curve fitting effectively eliminated noise in the curb results, enhancing the Precision, Recall, and F-1 score metrics to 0.8744, 0.8648, and 0.8696, respectively. Finally, the excellent detection performance and generalization of our proposed method were further verified in real scene experiments.

The 3D-Curb dataset and the CurbNet framework established in this study lay a foundation for future research in curb detection. In our upcoming research, we plan to create a more comprehensive dataset incorporating additional modalities. Similarly, we aim to explore and enhance the capabilities of the CurbNet framework, improving its performance in multi-modal data contexts.

REFERENCES

- [1] T. Luettel, M. Himmelsbach, and H.-J. Wuensche, “Autonomous ground vehicles—concepts and a path to the future,” *Proceedings of the IEEE*, vol. 100, no. Special Centennial Issue, pp. 1831–1839, 2012.
- [2] F. Ma, X. Yan, Y. Liu, and M. Liu, “Every dataset counts: Scaling up monocular 3d object detection with joint datasets training,” *arXiv preprint arXiv:2310.00920*, 2023.
- [3] Z. Xu, Y. Sun, and M. Liu, “icurb: Imitation learning-based detection of road curbs using aerial images for autonomous driving,” *IEEE Robotics and Automation Letters*, vol. 6, no. 2, pp. 1097–1104, 2021.
- [4] J. K. Suhr, J. Jang, D. Min, and H. G. Jung, “Sensor fusion-based low-cost vehicle localization system for complex urban environments,” *IEEE Transactions on Intelligent Transportation Systems*, vol. 18, no. 5, pp. 1078–1086, 2016.
- [5] A. Y. Hata, F. T. Ramos, and D. F. Wolf, “Monte carlo localization on gaussian process occupancy maps for urban environments,” *IEEE Transactions on Intelligent Transportation Systems*, vol. 19, no. 9, pp. 2893–2902, 2017.

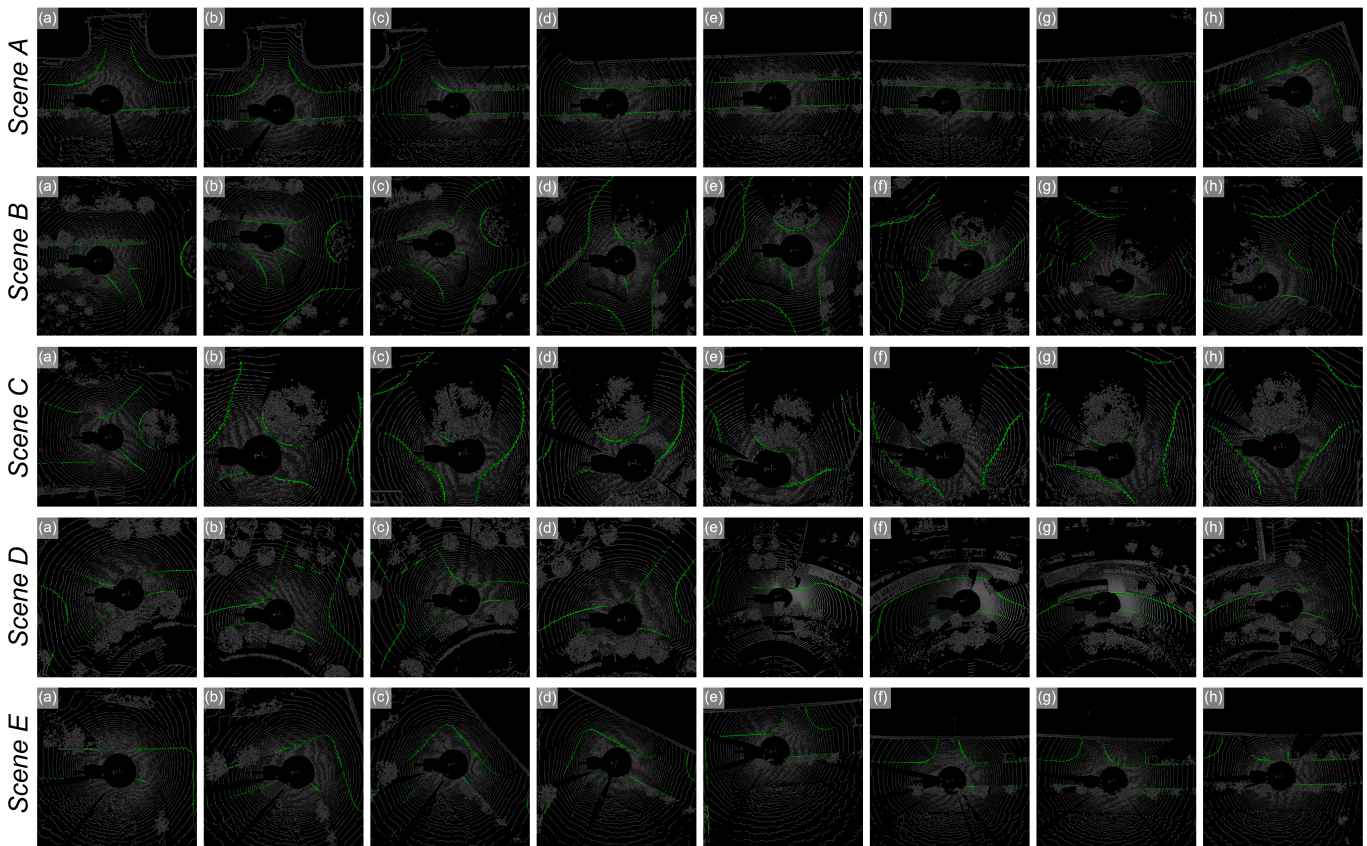


Fig. 10. **Curb detection results of real experiments in five field scenarios.** Our method achieves excellent curb detection results in five real-world scenarios. In particular, it also shows excellent performance in complex intersection scenarios B and C with irregular curb distribution.

- [6] L. M. Romero, J. A. Guerrero, and G. Romero, "Road curb detection: A historical survey," *Sensors*, vol. 21, no. 21, p. 6952, 2021.
- [7] A. B. Hillel, R. Lerner, D. Levi, and G. Raz, "Recent progress in road and lane detection: a survey," *Machine vision and applications*, vol. 25, no. 3, pp. 727–745, 2014.
- [8] C. Wei, H. Li, J. Shi, G. Zhao, H. Feng, and L. Quan, "Row anchor selection classification method for early-stage crop row-following," *Computers and Electronics in Agriculture*, vol. 192, p. 106577, 2022.
- [9] P. Sun, X. Zhao, Z. Xu, R. Wang, and H. Min, "A 3d lidar data-based dedicated road boundary detection algorithm for autonomous vehicles," *IEEE Access*, vol. 7, pp. 29 623–29 638, 2019.
- [10] F. Ma, S. Wang, and M. Liu, "An automatic multi-lidar extrinsic calibration algorithm using corner planes," in *2022 IEEE International Conference on Robotics and Biomimetics (ROBIO)*. IEEE, 2022, pp. 235–240.
- [11] F. Ma, Y. Liu, S. Wang, J. Wu, W. Qi, and M. Liu, "Self-supervised drivable area segmentation using lidar's depth information for autonomous driving," in *2023 IEEE/RSJ International Conference on Intelligent Robots and Systems (IROS)*. IEEE, 2023, pp. 41–48.
- [12] S. Ö. Demir, T. E. Ertop, A. B. Koku, and E. İ. Konukseven, "An adaptive approach for road boundary detection using 2d lidar sensor," in *2017 IEEE International Conference on Multisensor Fusion and Integration for Intelligent Systems (MFI)*. IEEE, 2017, pp. 206–211.
- [13] E. Horváth, C. Pozna, and M. Unger, "Real-time lidar-based urban road and sidewalk detection for autonomous vehicles," *Sensors*, 2021.
- [14] G. Wang, J. Wu, R. He, and B. Tian, "Speed and accuracy tradeoff for lidar data based road boundary detection," *IEEE/CAA Journal of Automatica Sinica*, vol. 8, no. 6, pp. 1210–1220, 2020.
- [15] T. Chen, B. Dai, D. Liu, J. Song, and Z. Liu, "Velodyne-based curb detection up to 50 meters away," in *2015 IEEE Intelligent Vehicles Symposium (IV)*. IEEE, 2015, pp. 241–248.
- [16] A. Y. Hata, F. S. Osorio, and D. F. Wolf, "Robust curb detection and vehicle localization in urban environments," in *2014 IEEE Intelligent Vehicles Symposium Proceedings*. IEEE, 2014, pp. 1257–1262.
- [17] L. Zhou and G. Vosselman, "Mapping curbstones in airborne and mobile laser scanning data," *International Journal of Applied Earth Observation and Geoinformation*, vol. 18, pp. 293–304, 2012.
- [18] S. Xu, R. Wang, and H. Zheng, "Road curb extraction from mobile lidar point clouds," *IEEE Transactions on Geoscience and Remote Sensing*, vol. 55, no. 2, pp. 996–1009, 2016.
- [19] Y. Zhang, J. Wang, X. Wang, and J. M. Dolan, "Road-segmentation-based curb detection method for self-driving via a 3d-lidar sensor," *IEEE transactions on intelligent transportation systems*, vol. 19, no. 12, pp. 3981–3991, 2018.
- [20] B. Qin, Z. Chong, T. Bandyopadhyay, M. H. Ang, E. Frazzoli, and D. Rus, "Curb-intersection feature based monte carlo localization on urban roads," in *2012 IEEE International Conference on Robotics and Automation*. IEEE, 2012, pp. 2640–2646.
- [21] G. Zhao, L. Quan, H. Li, H. Feng, S. Li, S. Zhang, and R. Liu, "Real-time recognition system of soybean seed full-surface defects based on deep learning," *Computers and Electronics in Agriculture*, vol. 187, p. 106230, 2021.
- [22] Z. Xu, Y. Sun, L. Wang, and M. Liu, "Cp-loss: Connectivity-preserving loss for road curb detection in autonomous driving with aerial images," in *2021 IEEE/RSJ International Conference on Intelligent Robots and Systems (IROS)*. IEEE, 2021, pp. 1117–1123.
- [23] Y. Jung, M. Jeon, C. Kim, S.-W. Seo, and S.-W. Kim, "Uncertainty-aware fast curb detection using convolutional networks in point clouds," in *2021 IEEE International Conference on Robotics and Automation (ICRA)*. IEEE, 2021, pp. 12 882–12 888.
- [24] T. Suleymanov, L. Kunze, and P. Newman, "Online inference and detection of curbs in partially occluded scenes with sparse lidar," in *2019 IEEE Intelligent Transportation Systems Conference (ITSC)*. IEEE, 2019, pp. 2693–2700.
- [25] J. Gao, H. Jie, B. Xu, L. Liu, J. Hu, and W. Liu, "Lcdet: Lidar curb detection network with transformer," in *2023 International Joint Conference on Neural Networks (IJCNN)*. IEEE, 2023, pp. 1–9.
- [26] J. L. Apellániz, M. García, N. Aranjuelo, J. Barandiarán, and M. Nieto, "Lidar-based curb detection for ground truth annotation in automated driving validation," *arXiv preprint arXiv:2312.00534*, 2023.
- [27] H. Zhou, X. Zhu, X. Song, Y. Ma, Z. Wang, H. Li, and D. Lin, "Cylinder3d: An effective 3d framework for driving-scene lidar semantic segmentation," *arXiv preprint arXiv:2008.01550*, 2020.
- [28] D. Zai, J. Li, Y. Guo, M. Cheng, Y. Lin, H. Luo, and C. Wang, "3-d road boundary extraction from mobile laser scanning data via supervoxels and

- graph cuts,” *IEEE Transactions on Intelligent Transportation Systems*, vol. 19, no. 3, pp. 802–813, 2017.
- [29] U. Ozertem and D. Erdogmus, “Locally defined principal curves and surfaces,” *The Journal of Machine Learning Research*, 2011.
- [30] H. Jie, J. Gao, Q. Zhao, Z. Ning, J. Hu, L. Liu, and W. Liu, “An efficient curb detection and tracking method for intelligent vehicles via a high-resolution 3d-lidar,” in *4th International Conference on Information Science, Electrical, and Automation Engineering (ISEAE 2022)*, vol. 12257. SPIE, 2022, pp. 310–317.
- [31] W. Yao, Z. Deng, and L. Zhou, “Road curb detection using 3d lidar and integral laser points for intelligent vehicles,” in *The 6th International Conference on Soft Computing and Intelligent Systems, and The 13th International Symposium on Advanced Intelligence Systems*. IEEE, 2012, pp. 100–105.
- [32] A. Y. Hata and D. F. Wolf, “Feature detection for vehicle localization in urban environments using a multilayer lidar,” *IEEE Transactions on Intelligent Transportation Systems*, vol. 17, no. 2, pp. 420–429, 2015.
- [33] B. Yang, L. Fang, and J. Li, “Semi-automated extraction and delineation of 3d roads of street scene from mobile laser scanning point clouds,” *ISPRS Journal of Photogrammetry and Remote Sensing*, vol. 79, pp. 80–93, 2013.
- [34] D. Bai, T. Cao, J. Guo, and B. Liu, “How to build a curb dataset with lidar data for autonomous driving,” in *2022 International Conference on Robotics and Automation (ICRA)*. IEEE, 2022, pp. 2576–2582.
- [35] J. Liang, N. Homayounfar, W.-C. Ma, S. Wang, and R. Urtasun, “Convolutional recurrent network for road boundary extraction,” in *Proceedings of the IEEE/CVF Conference on Computer Vision and Pattern Recognition*, 2019, pp. 9512–9521.
- [36] O. Ronneberger, P. Fischer, and T. Brox, “U-net: Convolutional networks for biomedical image segmentation,” in *Medical Image Computing and Computer-Assisted Intervention—MICCAI 2015: 18th International Conference, Munich, Germany, October 5–9, 2015, Proceedings, Part III 18*. Springer, 2015, pp. 234–241.
- [37] X. Pan, J. Shi, P. Luo, X. Wang, and X. Tang, “Spatial as deep: Spatial cnn for traffic scene understanding,” in *Proceedings of the AAAI Conference on Artificial Intelligence*, vol. 32, no. 1, 2018.
- [38] D. Kukolj, I. Marinović, and S. Nemet, “Road edge detection based on combined deep learning and spatial statistics of lidar data,” *Journal of Spatial Science*, vol. 68, no. 2, pp. 245–259, 2023.
- [39] H. Caesar, V. Bankiti, A. H. Lang, S. Vora, V. E. Liong, Q. Xu, A. Krishnan, Y. Pan, G. Baldan, and O. Beijbom, “nusenes: A multimodal dataset for autonomous driving,” in *Proceedings of the IEEE/CVF conference on computer vision and pattern recognition*, 2020, pp. 11 621–11 631.
- [40] A. Geiger, P. Lenz, C. Stiller, and R. Urtasun, “Vision meets robotics: The kitti dataset,” *The International Journal of Robotics Research*, vol. 32, no. 11, pp. 1231–1237, 2013.
- [41] J. Behley, M. Garbade, A. Milioto, J. Quenzel, S. Behnke, C. Stachniss, and J. Gall, “Semantickitti: A dataset for semantic scene understanding of lidar sequences,” in *Proceedings of the IEEE/CVF international conference on computer vision*, 2019, pp. 9297–9307.
- [42] H. Zhang, H. Zhang, C. Wang, and J. Xie, “Co-occurrent features in semantic segmentation,” in *Proceedings of the IEEE/CVF conference on computer vision and pattern recognition*, 2019, pp. 548–557.
- [43] W. Chen, X. Zhu, R. Sun, J. He, R. Li, X. Shen, and B. Yu, “Tensor low-rank reconstruction for semantic segmentation,” in *Computer Vision—ECCV 2020: 16th European Conference, Glasgow, UK, August 23–28, 2020, Proceedings, Part XVII 16*. Springer, 2020, pp. 52–69.
- [44] Z. Zhou, M. M. R. Siddiquee, N. Tajbakhsh, and J. Liang, “Unet++: Redesigning skip connections to exploit multiscale features in image segmentation,” *IEEE transactions on medical imaging*, vol. 39, no. 6, pp. 1856–1867, 2019.
- [45] S. Jadon, “A survey of loss functions for semantic segmentation,” in *2020 IEEE conference on computational intelligence in bioinformatics and computational biology (CIBCB)*. IEEE, 2020, pp. 1–7.
- [46] E. Schubert, J. Sander, M. Ester, H. P. Kriegel, and X. Xu, “DbSCAN revisited, revisited: why and how you should (still) use dbSCAN,” *ACM Transactions on Database Systems (TODS)*, 2017.
- [47] A. H. Lang, S. Vora, H. Caesar, L. Zhou, J. Yang, and O. Beijbom, “Pointpillars: Fast encoders for object detection from point clouds,” in *Proceedings of the IEEE/CVF conference on computer vision and pattern recognition*, 2019, pp. 12 697–12 705.
- [48] Z. Liu, Y. Lin, Y. Cao, H. Hu, Y. Wei, Z. Zhang, S. Lin, and B. Guo, “Swin transformer: Hierarchical vision transformer using shifted windows,” in *Proceedings of the IEEE/CVF international conference on computer vision*, 2021, pp. 10 012–10 022.

- [49] X. Dong, J. Bao, D. Chen, W. Zhang, N. Yu, L. Yuan, D. Chen, and B. Guo, “Cswin transformer: A general vision transformer backbone with cross-shaped windows,” in *Proceedings of the IEEE/CVF Conference on Computer Vision and Pattern Recognition*, 2022, pp. 12 124–12 134.
- [50] Ö. Çiçek, A. Abdulkadir, S. S. Lienkamp, T. Brox, and O. Ronneberger, “3d u-net: learning dense volumetric segmentation from sparse annotation,” in *Medical Image Computing and Computer-Assisted Intervention—MICCAI 2016: 19th International Conference, Athens, Greece, October 17–21, 2016, Proceedings, Part II 19*. Springer, 2016, pp. 424–432.

VII. BIOGRAPHY SECTION



Guoyang ZHAO (Student Member, IEEE) is currently pursuing a Master of philosophy degree in the Intelligent Autonomous Driving Center, Thrust of Robotics and Autonomous Systems, The Hong Kong University of Science and Technology, Guangzhou, China. His research interests include computer vision, robotics, and deep learning.



Fulong Ma (Member, IEEE) received the B.E degree in automation from University of Science and Technology of China, Hefei, China, in 2018. He is currently pursuing the Ph.D degree with the Thrust of Robotics and Autonomous Systems, The Hong Kong University of Science and Technology, Guangzhou, China. His research interests include computer vision, sensor calibration, and deep learning.



Yuxuan Liu (Student Member, IEEE) received his Bachelor’s degree from Zhejiang University, Zhejiang, China in 2019, majoring in Mechatronic. He is now a Ph.D candidate at the Department of Electronic and Computer Engineering, The Hong Kong University of Science and Technology, Hong Kong, China. His current research interests include autonomous driving, deep learning, robotics, visual 3D object detection, visual depth prediction, etc..



Weiqing Qi received his Bachelor’s degree from University of California, Santa Barbara in 2021, majoring in Computer Science. He is currently pursuing the Master of philosophy degree with the Thrust of Robotics and Autonomous Systems, The Hong Kong University of Science and Technology, Hong Kong, China. His current research interests include lane detection, drivable area segmentation, and semantics segmentation, etc.



Ming Liu (Senior Member, IEEE) received the B.A. degree in automation from Tongji University, Shanghai, China, in 2005, and the Ph.D. degree from the Department of Mechanical and Process Engineering, ETH Zürich, Zürich, Switzerland, in 2013. During his master’s degree with Tongji University, he stayed one year at Erlangen-Nürnberg University, Erlangen, Germany, and the Fraunhofer Institute IISB, Erlangen, as a Master Visiting Scholar. He is currently an Associate Professor with the Department of Electronic and Computer Engineering, the Department of Computer Science and Engineering, and the Cheng Kar-Shun Robotics Institute, The Hong Kong University of Science and Technology, Hong Kong. His research interests include dynamic environment modeling, deep learning for robotics, 3-D mapping, machine learning, and visual control..